

Article

Model Experiment Study on Vertical Bearing Characteristics of Large-Diameter Ring Piles

Yingtao Sun ^{1,*} , Aijun Yao ¹, Lei Dong ², Yanlin Li ¹  and Yifei Gong ¹

¹ Institute of Geotechnical and Underground Engineering, Beijing University of Technology, Beijing 100124, China

² Institute of Geotechnical and Underground Engineering, China Railway Construction Group Co., Ltd., Beijing 100040, China

* Correspondence: sunyingtao218@163.com

Abstract: The hollow structure of large-diameter ring piles (LDRPs) reduces the amount of concrete used, is economically efficient, and reduces the weight of the pile. However, its bearing characteristics and safety performance are still not fully known. In this study, to determine the properties of the LDRP structure, a combination of the indoor scale model test and numerical simulations was used, and a new parameter, K , which is the thickness-to-diameter ratio, was introduced. A comparative study of LDRPs with different hollow ranges was conducted. The results show that for a value of K in the range of 0.2–1, the ultimate bearing capacity of LDRPs is not significantly different from that of large-diameter solid piles (LDSPs), and they can ensure sufficient safety reserves. Under ultimate bearing capacity, the strain on an LDRP is large, but it does not exceed its own material strength, and the strain variation law is similar to that of a solid pile. LDRPs show the characteristics of end-bearing piles, and concrete savings can reach up to 50% for K in the range of 0.2–1.

Keywords: model experiment; thickness-to-diameter ratio; large-diameter ring pile; bearing characteristics



Citation: Sun, Y.; Yao, A.; Dong, L.; Li, Y.; Gong, Y. Model Experiment Study on Vertical Bearing Characteristics of Large-Diameter Ring Piles. *Appl. Sci.* **2022**, *12*, 13011. <https://doi.org/10.3390/app122413011>

Academic Editor: Cheng-Yu Ku

Received: 21 October 2022

Revised: 14 December 2022

Accepted: 16 December 2022

Published: 18 December 2022

Publisher's Note: MDPI stays neutral with regard to jurisdictional claims in published maps and institutional affiliations.



Copyright: © 2022 by the authors. Licensee MDPI, Basel, Switzerland. This article is an open access article distributed under the terms and conditions of the Creative Commons Attribution (CC BY) license (<https://creativecommons.org/licenses/by/4.0/>).

1. Introduction

With the rapid development of science and technology, the demand for buildings has also substantially increased. Ordinary low-rise buildings have been unable to meet the needs of urban development. High-rise and super-high-rise buildings have become the new trend in urban construction. However, the increase in upper load puts forward higher requirements for the bearing capacity of the lower foundation. Pile foundations have the advantages of good seismic performance, high ultimate bearing capacity, and low construction noise; hence, they have been widely used in urban buildings.

The large-diameter ring pile (LDRP) is a special pile type among many different pile foundations. Compared with the traditional large-diameter solid pile (LDSP), the external contour of the LDRP body is not very different. The biggest difference is the hollow structure of the annular pile. Its construction process generally involves excavating a large-diameter circular hole, followed by setting up a steel plate mold to form a hollow structure, and finally pouring concrete around the mold. The special hollow structure of the LDRP reduces the amount of concrete used, thereby reducing the self-weight and additional stress on the foundation and improving the bearing capacity. Therefore, it has better adaptability to some special strata, such as in the Shenzhen Bridge in China. During its construction process, well-developed karst caves were found in the lower part of the stratum. When the drilling depth reached 80 m, no stable soil layer that could be used as a bored pile was found. The shortest horizontal distance between the original design pier and adjacent railway was only 1.6 m. Consequently, the original design was changed to include two large step-tapered hollow piles with diameters of 14 m and 15 m, and the buried depth was 16 m. With these modifications, the construction was successfully completed. Based on this project,

Song Jiang (2020) [1] and Ming Huang et al. (2020) [2] combined numerical simulation experiments, theoretical analysis, and field measurement to show the superiority of large step-tapered hollow piles and proposed the analytical solution for this pile foundation settlement. Yunxiu Dong's (2019) [3] research on large-diameter hollow composite piles shows that the bearing capacity of large-diameter hollow composite pile foundations is 19.1% higher than that of solid pile groups with the same side area. In addition, in terms of seismic performance, Yongmou Zhang (2011) [4] demonstrated that hollow piles are superior to solid piles by comparing the deflections, rotation angles, bending moments, and shear forces of hollow piles and solid piles with the same cross-sectional area.

In the field of pile foundation, the most important things are its settlement law and load-transfer mechanisms, but most of the research is based on large-diameter solid piles. For example, Ruan Xiang (2017) [5] proposed a practical algorithm for the bearing capacity of large-diameter pile ends based on displacement control and the Mindlin solution for the load stress distribution in the semi-infinite space. This method considers the belled diameter, embedded depth, thickness of the bearing, and soft substratum. The calculation results of the influence of physical and mechanical properties on the bearing capacity are consistent with the actual project. Si Xiao (2018) [6] studied the longitudinal coupling vibration of large-diameter end-bearing piles in saturated soil and analyzed the influence of the pile slenderness ratio on the transverse inertia effect of piles based on the saturated soil theory proposed by Biot and the Rayleigh–Love rod, considering the transverse inertia effect. The results show that the transverse inertia effect should be considered in the low-strain integrity test of large-diameter piles, and the Poisson's ratio, slenderness ratio, and pile–soil modulus ratio have a significant effect on the transverse inertia effect of large-diameter piles, while the seepage force of saturated soil has little effect. To meet engineering needs, considering the transverse inertia effect of large-diameter piles is a necessary condition. Taking the load-transfer curve of large-diameter single piles as the object, H. Wang (2020) [7] quantified the relationship between pile diameters and their bending stiffness in sand and established a relationship with the p – y curve for lateral load. With an increase in pile diameter, the correction of the p – y curve is mainly related to the change in the soil deformation mechanism around the pile. The influence of surface friction, foundation shear force, and foundation moment of large-diameter piles on the p – y curve was almost negligible. A new p – y curve was proposed with better predictions for large-diameter piles. Raymond Mankbadi (2010) [8] showed that the dynamic load test for large-diameter open concrete piles is limited and frequently underestimates pile-bearing capacity. Therefore, static load tests are recommended, whose results should be combined with those of dynamic load tests to promote the design and construction of large-diameter piles. Liu Xueying (2020) [9] and Hui Yang et al. (2013) [10] clarified the load-transfer mechanism of large-diameter rock-socketed piles and determined the performance characteristics of ultimate end resistance and ultimate side resistance. The pile-end resistance increases linearly with the settlement of the pile end, and the rock ultimate side resistance coefficient of the rock-socketed section has no significant correlation with the pile diameter of the rock-socketed section. However, the ultimate resistance coefficient increases with an increase in pile diameter. However, when the pile diameter is less than 1000 mm, the correlation is not obvious. On the pile diameter problem, W. D. Liam (2016) [11] also proposed a different method to evaluate the pile diameter effect for the finite element simulation software. The commonly used LPILE program ignores the volume of the pile, and the results are ideal when the deflection is less than 60 mm. However, after more than 60 mm, the load displacement curve will diverge, and the analysis results will not accurately represent the interaction between the pile and the soil. Therefore, it is necessary to calibrate the data according to the static load experiment to deal with the unreliability of the p – y curve.

The existing research has revealed the settlement mechanisms and mechanical properties of pile foundations in detail from both theoretical and practical perspectives, making significant contributions to the field of pile foundation. However, the mechanical properties

of LDRPs and whether they have similar physical and mechanical properties to LDSPs must still be determined. The hollow part is the key structure of LDRPs, and the effect of the size of the hollow on the overall mechanical properties of the pile must be determined. The appropriate size that not only ensures the ultimate bearing capacity of the pile but also reduces the use of concrete and provides economic benefits is of great interest. In view of the above problems, we adopted the method of combining a scale vertical static load model with numerical simulations and introduced a new parameter, the thickness-to-diameter ratio, K , to quantitatively distinguish between five LDRPs with the same pile diameter but different hollow ranges. The overall mechanical properties of LDRPs are revealed from the perspectives of pile settlement, pile stress, and pile strain. The range of the thickness-to-diameter ratio, K , given in the conclusion, provides a new reference for the design and applications of LDRPs in the future.

2. Model Experiment Design

The model parameters are based on the project of the Tsinghua Experimental Base in Beijing, China, which intends to build an LDRP with a diameter of 10 m and a length of 33 m. The size similarity coefficient of the model test was determined to be 20:1.

A new parameter, K , was introduced as the classification basis for ring piles. K is defined as the ratio of the wall thickness (T) of an LDRP to the pile radius (R). The specific formula is given in (1). Figure 1 shows the cross-section of a pile body, such as an LDRP. This parameter can directly represent the proportion of the hollow part of the ring pile. For a solid pile, $K = 1$, and the smaller the K value, the smaller the wall thickness and the larger the proportion of the hollow part.

$$K = T/R \quad (1)$$

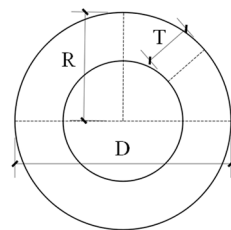


Figure 1. Cross-section of pile body.

In this experiment, K was taken as the main reference and concrete savings as the secondary reference. A total of 5 groups of model pile tests were set up (as shown in Table 1). Concrete with the same specifications as the original project was selected as the material for the model pile, with an elastic modulus of $E = 3.0 \times 10^4$ MPa and a reinforcement cage of uniform size. The bottom of the model pile was a 300 mm concrete seal. The pile strength measured 28 days after pouring and curing was 30 MPa. The only difference in the model piles was the difference in the hollow ranges, i.e., the difference in K . Figure 2 shows the cross-section of the pile model.

Table 1. Model pile's specifications.

Project	Outer Diameter D/mm	Inner Diameter d/mm	Wall Thickness T/mm	Pile Length/mm	Thickness to Diameter Ratio K	Concrete Savings
Solid Pile No. 1	500	0	250	1670	1	0%
Ring Pile No. 2	500	200	150		0.6	16%
Ring Pile No. 3	500	300	100		0.4	36%
Ring Pile No. 4	500	360	70		0.28	52%
Ring Pile No. 5	500	400	50		0.2	64%

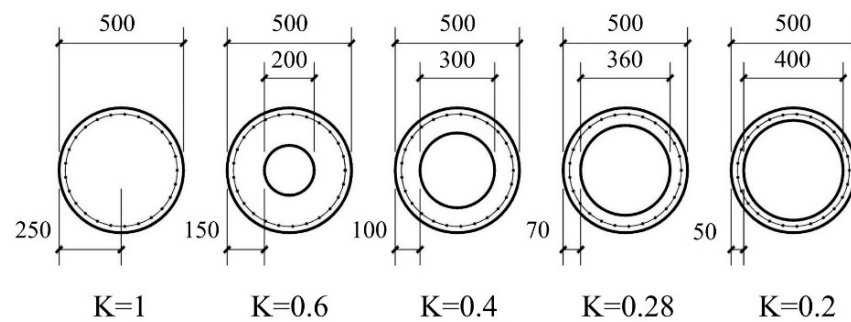


Figure 2. Cross-section of pile model (from left to right: No.1, No. 2, No. 3, No. 4, No. 5).

The model box was designed as a steel tube (2200 mm in height and 1000 mm in diameter) formed by bending a steel plate. The tubular model box can better maintain the stress field in the soil and prevent the dissipation of the Chow ring stress in the pile during the experiment.

According to geological exploration data, at the original project site, within a 36 m depth range, the soil type was a gravel layer mixed with sand. Therefore, in the experiment, we used a soil layer with 10–20 mm of gravel and fine sand, mixed in the ratio of 2:3 (Figure 3). The relationship between relative density and the free fall of sand particles, as mentioned in Plaban Deb (2020) [12], is shown in Figure 4, where sand particles falling from a height of 520 mm resulted in a soil bed with a relative density of 70%. The height of the model box for this experiment was 2200 mm. First, soil was poured into the box, using the sand-pouring method. At every 200 mm in depth, the soil was compacted by using artificial vibrations. By following this procedure, soils in the model box with relative densities greater than 90% can be obtained, and the uniformity of the relative densities of the soils can be ensured.



Figure 3. Model soil.

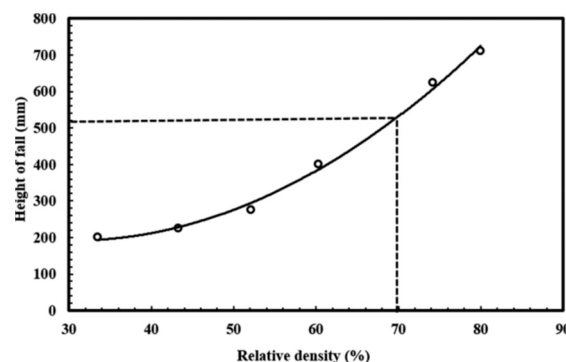


Figure 4. Variation of relative density of sand with the height of free fall (Plaban Deb, 2020) [12].

The bottom of the model box was first paved with 500 mm of soil, which was the bearing soil at the end of the pile. Then the model pile was placed and filled with soil. The model piles were rearranged in the same way after every replacement.

The ultimate bearing capacity of the prototype pile is 389,169 kN. According to the dimension similarity coefficient, $C_L = 20:1$, the estimated load of the model pile is 48 kN. A 10-stage loading process was therefore designed to be applied at a rate of 20 kN/h at 10 kN per stage and maintained for 1 h until the pressure sensor monitoring data remained stable and the loading continued. The purpose of this experiment was to investigate the mechanical properties of LDRPs under vertical load. Two times the limit load can help establish the complete load–settlement curve and stress–strain relationship to reveal the laws of mechanical change in the whole process. The experimental device diagram is depicted in Figure 5, and the experimental site is shown in Figure 6. The sampling frequencies of the displacement sensor and strain sensor are 1 Hz and 0.1 Hz, respectively. The data within 10 min before the first stage of loading were taken and analyzed.

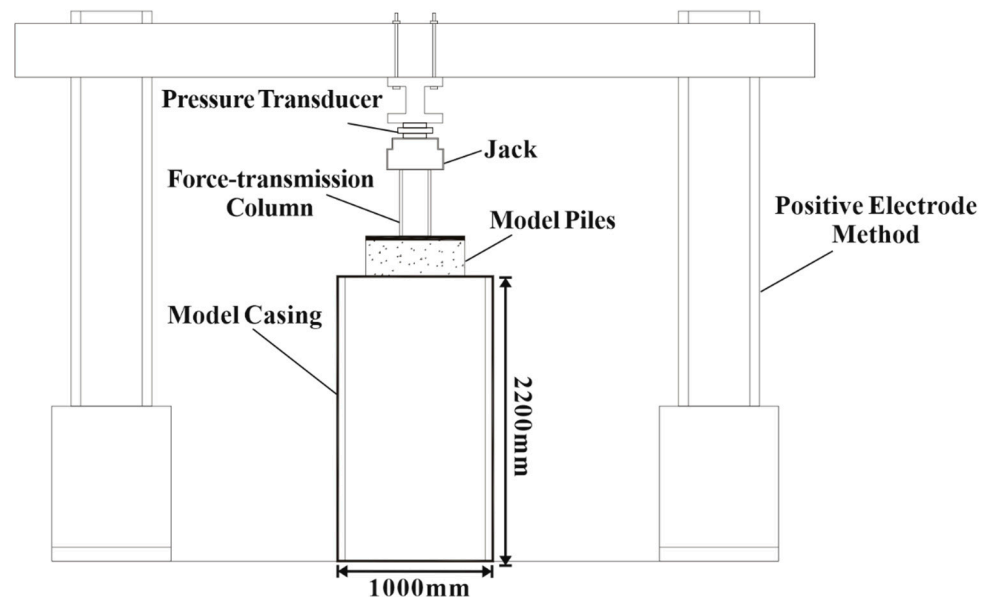


Figure 5. Schematic of the experimental device.

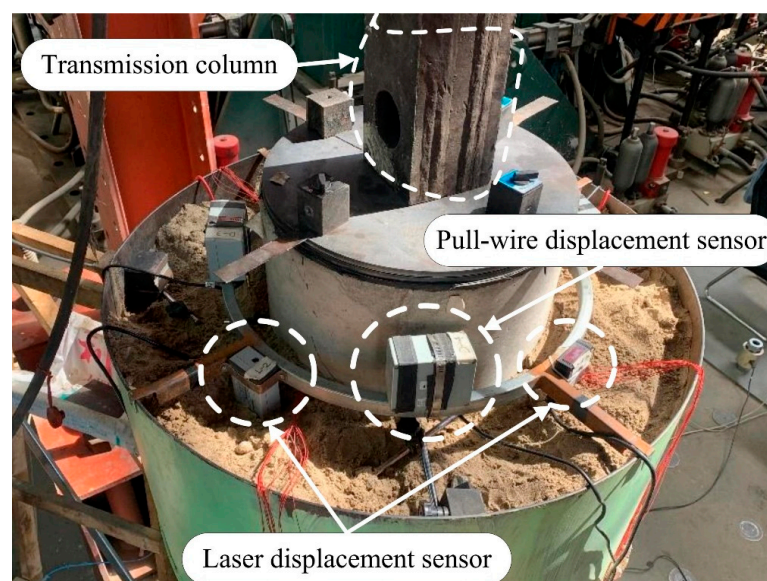


Figure 6. Experimental site.

3. Analysis of Model Experimental Results

3.1. Analysis of Settlement Law of Pile Top and Pile Bottom in Model Experiment

The Q_{top} - s curve of the pile top and Q_{bottom} - s curve of the pile bottom are shown in Figures 7 and 8, respectively.

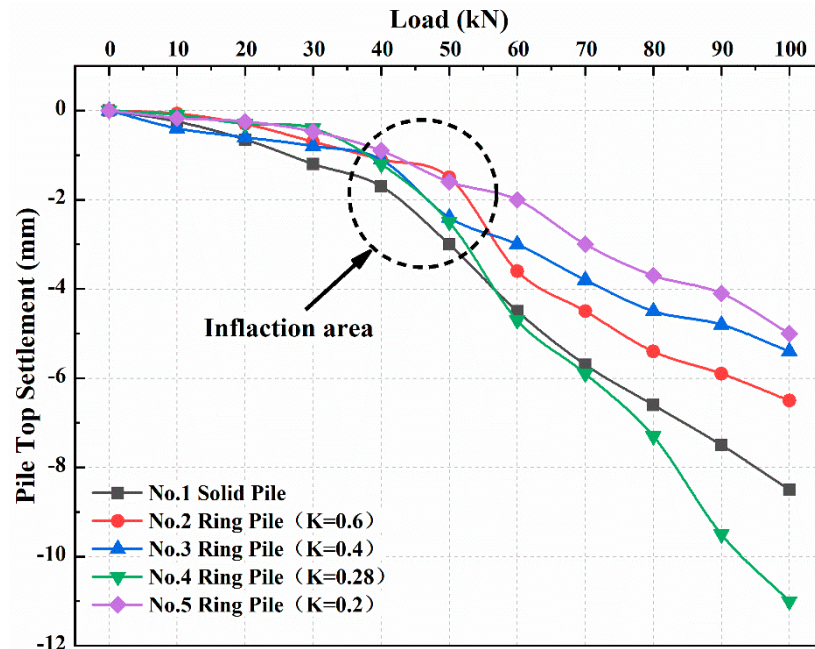


Figure 7. The settlement of pile top.

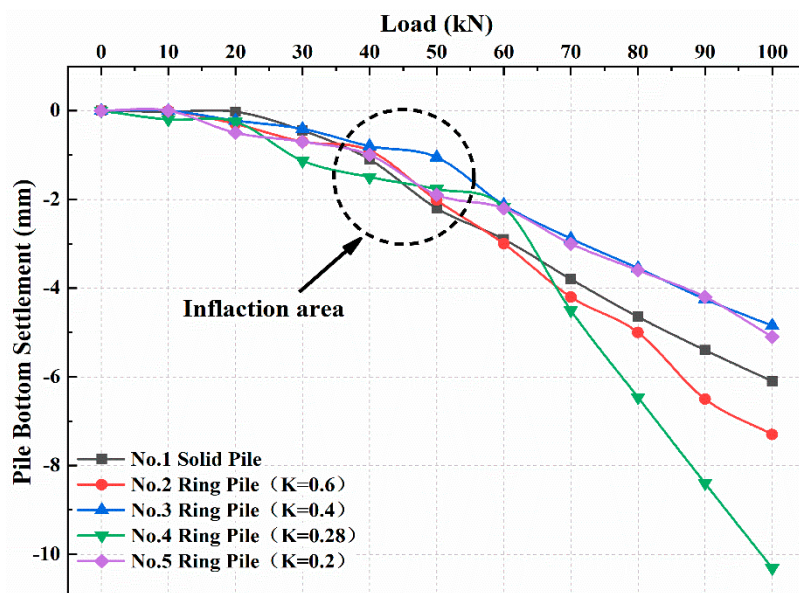


Figure 8. The settlement of pile bottom.

Two methods to determine the ultimate bearing capacity of a single pile are stipulated in China’s *GB50007-2011 Code for the Design of Building Foundations* [13]:

- (1) When the load–settlement curve suddenly changes from a slow drop at the beginning to a steep drop, the load corresponding to the initial point of the curve’s steep drop can be considered the ultimate bearing capacity of the pile.

- (2) If no obvious change in the load–settlement curve is observed and the overall trend is a slow decline, then the load corresponding to the settlement of 40 mm can be regarded as the ultimate bearing capacity of the pile.

In this experiment, obvious inflection points were observed in the settlement curves of the pile top and pile bottom of the five model piles. The inflection points are concentrated in the load range of 40–55 kN. In this range, the settlement of the pile body changed from a gentle increase to a steep increase. Therefore, the load at the inflection point is the ultimate bearing capacity of the pile body.

Because pile top settlement directly affects the superstructure, it is taken as the main reference index. As shown in Figure 7, from the beginning of the loading to 20 kN, the settlement of the pile body was small and had no obvious change. The settlement of the pile tops of the five piles was approximately 0.5 mm. The settlement increased gradually when the load increased to 40 kN. An inflection point appeared between 40 and 55 kN, at which point we considered the pile foundation to be destroyed. When the upper load continues to increase, the settlement after the inflection point begins to increase significantly. The maximum settlement amount of the pile body was 10 mm at 100 kN. A comparison of pile settlements for different model piles is shown in Table 2.

Table 2. Comparison of settlement of model piles.

Model Pile	Outer Diameter D/mm	Wall Thickness T/mm	K	Ultimate Bearing Capacity/kN	Settlement under Ultimate Bearing Capacity	
					Pile Top /mm	Pile Bottom /mm
Solid Pile No. 1	500	250	1	50	−2.2	−2
Ring Pile No. 2	500	150	0.6	50	−2.4	−2.02
Ring Pile No. 3	500	100	0.4	50	−2.4	−1.7
Ring Pile No. 4	500	70	0.28	40	−1.2	−1.5
Ring Pile No. 5	500	50	0.2	40	−0.9	−1

Combining the data in Table 2 with those in Figure 7, when the outer diameter of the pile is the same and the bottom of the pile is covered, a small difference is observed in the ultimate bearing capacity of LDRPs and LDSPs, with $K = 0.2–1$, set in this test. For Ring Pile No. 5, with the least favorable $K = 0.2$, only 36% of the concrete content of the solid pile can attain 80% of the ultimate bearing capacity of the solid pile. In addition, pile safety is clearly stipulated in “GB50007-2011 Code for Design of Building Foundation” [13], approved and issued by the Ministry of Construction of the People’s Republic of China. The vertical ultimate bearing capacity of a single pile is divided by a safety factor of 2, which is the characteristic value R_a of the vertical bearing capacity of a single pile. This characteristic value will be used as the actual engineering design standard. The characteristic values of the bearing capacities of Solid Pile No. 1 and Ring Pile No. 5 are shown in Table 3.

Table 3. Comparison of characteristic values of ultimate bearing capacity.

Project	No. 1 Solid Pile	No. 5 Ring Pile
Ultimate bearing capacity	50 kN	40 kN
Safety factor	2	
Characteristic value of ultimate bearing capacity	25 kN	20 kN
Safety reserve	25 kN (100%)	20 kN (100%)
Pile safety reserve under 25 kN	25 kN (100%)	15 kN (75%)

As shown in Table 3, considering the most unfavorable situation, Ring Pile No. 5 was subjected to the load of the characteristic value of the bearing capacity of Solid Pile No. 1 and still had 75% safety reserve.

3.2. Analysis of Pile Compression Law in Model Experiment

The compression–load curve (Figure 9) can be obtained by extracting the data within 30 min before the load changes and taking the average value. The pile wall thickness has a significant impact on pile compression. The general rule is that the smaller the value of K , the smaller the wall thickness, T , and the greater the compression amount.

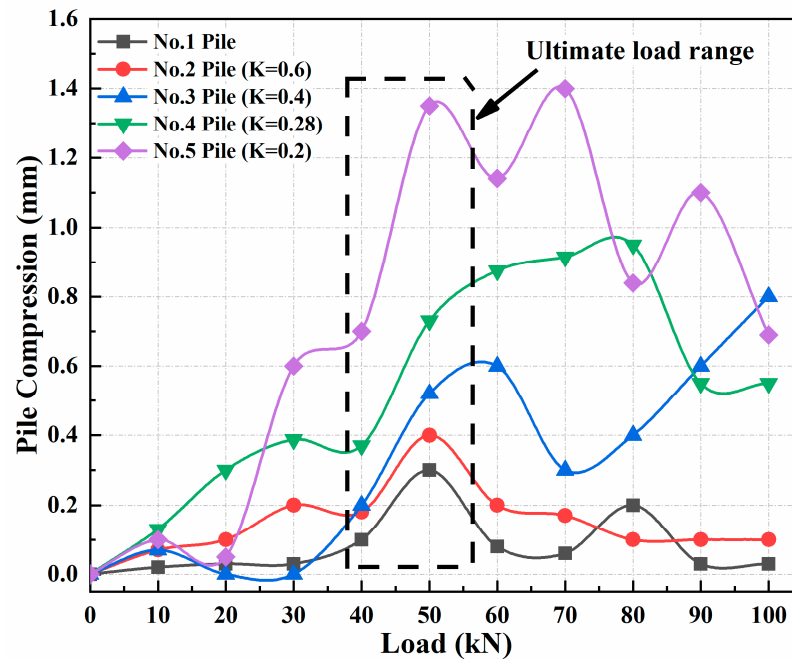


Figure 9. Pile compression curve.

The compression of Ring Pile No. 4 was slightly larger, at 10 kN, whereas the compression of the other four piles was small, less than 0.1 mm. The compression of Ring Pile No. 2 changed slightly when the load increased to 30 kN, reaching 0.4 mm.

The compression of the five piles increased significantly, within the inflection point range, at a load of 40 kN.

The total settlement of a single pile consists of the compression of the pile subsoil and compression of the pile body. The pile body does not undergo large compression, owing to the structure and material strength of the traditional solid pile. Because the inner wall of the ring pile is against an empty space and the cross-sectional area of the pile body under stress is small, pile body compression is more likely to occur.

Table 4 shows the pile compression within the inflection point range. Obvious anomalies were observed in the data of Ring Pile No. 2, and these points were excluded from the analysis. Within the load range of the inflection point, the pile compression increased gradually as the value of K decreased. However, the compression remained less than 0.8 mm as the load increased to 60 kN. In addition to Ring Pile No. 4, the other four piles reached their peak displacement. As the load increased further, the pile-end bearing capacity and pile-side friction reached their maximum limits, and pile-end pierce damage occurred; the soil at the pile endpoint compressed rapidly, and stress was released to the surrounding soil. Then pile compression tended to decrease.

Table 4. Comparison of compression in model piles.

File Type	Solid Pile No. 1	Ring Pile No. 2	Ring Pile No. 3	Ring Pile No. 4	Ring Pile No. 5
Compression under 40 kN/mm	0.1	0.18	0.2	0.4	0.7
Compression under 50 kN/mm	0.3	0.4	0.52	0.73	1.35
K	1	0.6	0.4	0.28	0.2

3.3. Analysis of Pile Strain Law in Model Experiment

The pile strain was also an important factor in this experiment. Under the same load, stressed structures with different volumes will inevitably produce strains of different magnitudes. The magnitude and law of strain have a significant impact on the evaluation of pile quality when using the parameter K.

In this experiment, all the measured pile-strain values were micro-strains.

Figures 10–15 show the pile body strains of the five piles. Under the ultimate load of the pile, the strain of Ring Pile No. 5 had an obvious separation degree, and the value of the strain was much higher than that of other piles. Compared with the solid pile, the overall strain of the ring pile was higher than that of the solid pile. The strain at the pile top was slightly larger. From the top to the middle of the pile, the strain tended to decrease with the increase in depth, reaching a minimum at the middle position of the pile and increasing thereafter. The closer a point is to the bottom of the pile, the greater the strain at that point. However, the strain decreased slightly at the bottom of the pile.

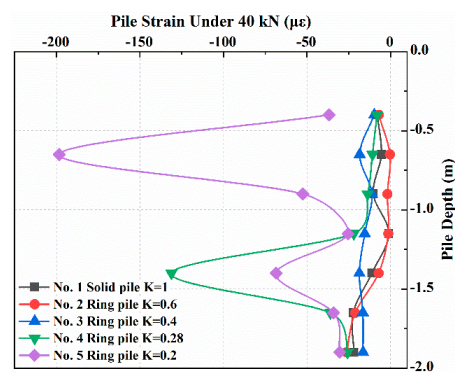


Figure 10. Pile strain under 40 kN.

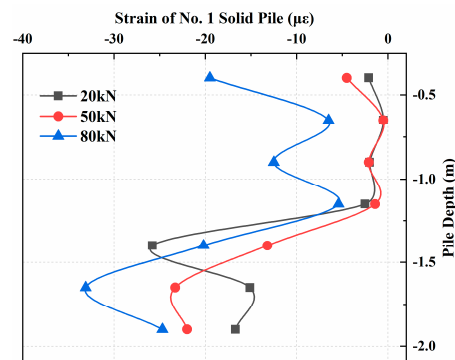


Figure 11. Pile strain of Solid Pile No. 1.

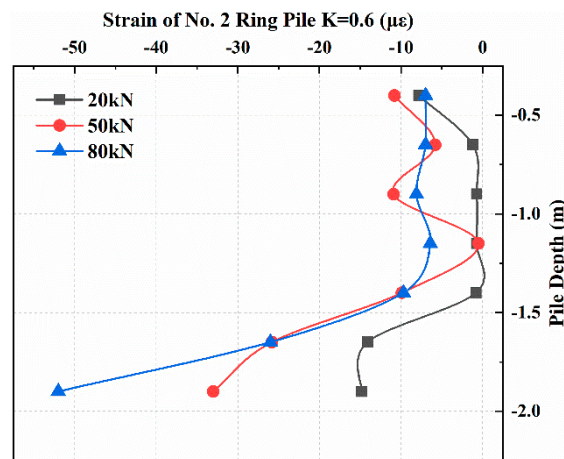


Figure 12. Pile strain of Solid Pile No. 2.

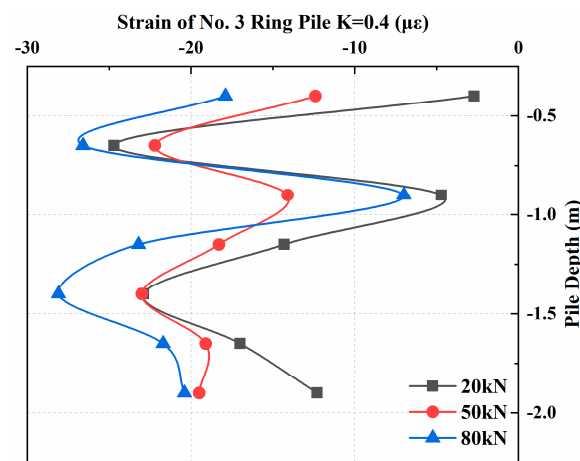


Figure 13. Pile strain of Ring Pile No. 3.

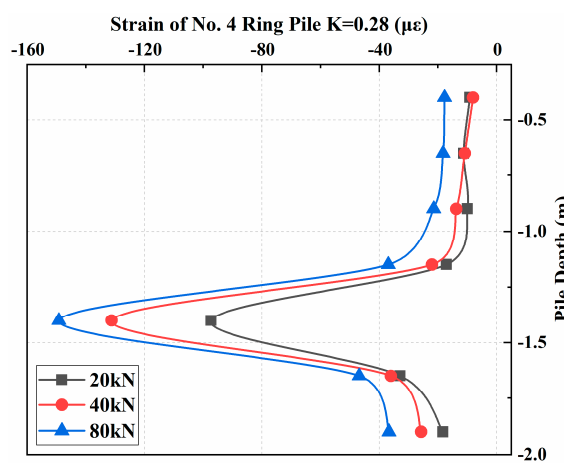


Figure 14. Pile strain of Ring Pile No. 4.

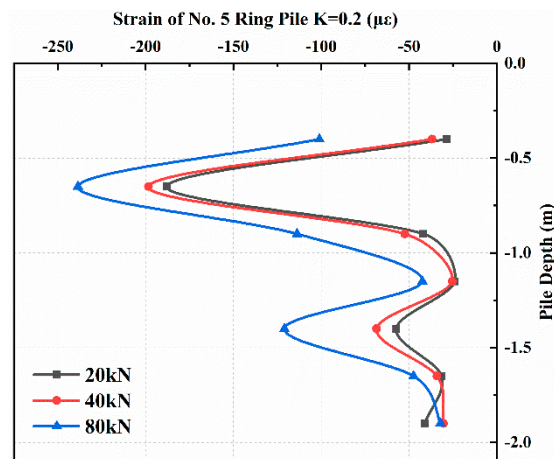


Figure 15. Pile strain of Ring Pile No. 5.

In the experiment, the strain gauge was attached to the pile surface, and the strain gauge at the bottom of the pile was close to the edge. The confined soil at the bottom of the pile was sand with low relative strength, which could be regarded as a weak cushion. In addition, because the pile bottom was flat, the stress distribution was uniform, with a small strain value. However, part of the strain gauge at the bottom edge of the pile will inevitably press small stones, resulting in stress concentration and strain increase. As shown in Figure 12, there was a sudden increase of strain at the bottom.

The strain development law of the four ring piles with different wall thicknesses was similar to that of the solid piles. A general law was observed: the smaller the value of K , the larger the strain at the top of the pile. The strain at the top of Ring Pile No. 5 was significantly larger and was five times that of other piles under the same load.

At approximately 0.75 m away from the pile top, with a variation in the value of K , strain growth showed a large variation: The change in strain growth of Ring Pile No. 2 ($K = 0.6$) was similar to that of the solid pile but decreased or increased slightly. The strains of Ring Pile No. 3 ($K = 0.4$) and Ring Pile No. 5 ($K = 0.2$) showed an obvious surge at this point, whereas the strain of Solid Pile No. 5 was approximately ten times that of the other piles.

At the middle position of the pile, the strains of all four ring piles decreased by different amounts. After passing through the middle position, the strains of the four ring piles and solid piles increased with depth. At approximately 0.4 m away from the pile bottom, the strain decreased gradually.

A 300 mm seal was placed at the bottom of the pile. Because the cross-sectional area of the pile and stressed area increased, the strain in this part decreased.

In addition, the peak point of the pile strain curve indicates that, with the decrease in the value of K , the position of the maximum pile strain gradually moved up. The pile depth corresponding to the peak strain value is shown in Table 5.

Table 5. The position and size of the peak strain of the pile body.

Piles	Solid Pile No. 1	Ring Pile No. 2	Ring Pile No. 3	Ring Pile No. 4	Ring Pile No. 5
K	1	0.6	0.4	0.28	0.2
Maximum strain position/m	-1.65	-1.65	-0.5	-0.92	-0.5
Strain value/ $\mu\epsilon$	-40	-65	-35	-175	-254

When the settlement and bearing capacity of the pile meet the requirements, the material strength of the pile must also be evaluated. Table 6 shows the relevant parameters of the concrete material of the model pile.

Table 6. Related parameters of C30 concrete.

Project	Elastic Modulus E/MPa	Poisson’s Ratio	Standard Value of Compressive Strength f_{ck} /MPa	Design Value of Compressive Strength f_c /MPa
Concrete	3.0×10^4	0.3	23.5	14.3

When the strain is converted into stress, if the stress is less than the design value of the concrete’s compressive strength, then the pile will not be damaged by material. The relevant results are shown in Table 7.

Table 7. Stresses corresponding to the peak strain of the piles.

Pile Type	Solid Pile No. 1	Ring Pile No. 2	Ring Pile No. 3	Ring Pile No. 4	Ring Pile No. 5
Maximum strain	−40	−65	−35	−175	−254
Maximum stress	1.2 MPa	1.95 MPa	1.05 MPa	5.15 MPa	7.62 MPa
Concrete strength		$f_{ck} = 23.5$ MPa		$f_c = 14.3$ MPa	
K	1	0.6	0.4	0.28	0.2

As shown in Table 7, the peak stress of the five piles is far less than the strength of the material. The pile body will not be damaged because of insufficient material strength. According to the similarity theory and stress–strain similarity coefficient of 1:1, the pile body will not be damaged when restored to the actual project. Therefore, we can conclude that LDRPs meet the safety index.

Excluding the error owing to Ring Pile No. 2 data and comparing the results with those of the other four piles, the peak stress of the pile increased significantly with a decrease in the value of K. When K decreased from 0.4 to 0.28, the stress increased up to 300%; however, when K was less than 0.4, the fluctuation in pile stress was small.

4. Numerical Simulations for Verification

To verify the accuracy of the model experiments, three sets of numerical simulation experiments were designed and implemented.

In the numerical simulation experiment scheme, the solid pile; Ring Pile No. 3; and the most unfavorable ring pile, Ring Pile No. 5, were selected as references and designed according to the original project size. The specific experimental scheme is shown in Table 8.

Table 8. Input parameters for the numerical simulations.

Project	Outer Diameter D/m	Inner Diameter/m	Wall Thickness T/m	K	Concrete Savings
Solid Pile No. 1	10	0	5	1	0%
Ring Pile No. 3	10	6	2	0.4	36%
Ring Pile No. 5	10	8	1	0.2	64%

Numerical simulations were performed by using Midas GTX NX finite element numerical simulation software, according to pile diameter and pile length. To avoid the boundary effect, a soil model with 10 times the pile diameter, that is, with a size of 100 m × 100 m × 100 m, was established (Yaru Lv, 2017) [14]. According to the original engineering geological survey, the model constituted seven soil layers, and finite element calculations were carried out by using the Mohr–Coulomb soil constitutive model. Model piles are elastic constitutive models. Figure 16 shows the results of the numerical simulations conducted on the model. Except for the top surface, which was free, the remaining surfaces were not allowed to produce displacement. The material of the model piles is the same as the original project and is regarded as an elastic

constitutive model. In the meshing process, using a small volume grid yields more accurate and detailed calculation results. However, refining the grid of the entire model was not necessary. Therefore, the grid sizes of the pile body and boundary were in the ratio 1:5. (Anup Sinha, 2016; Plaban Deb, 2022) [15,16].

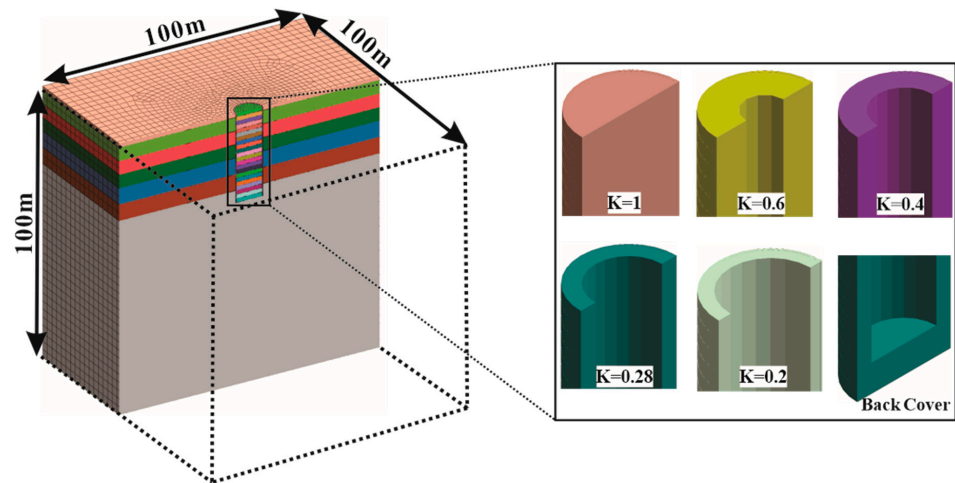


Figure 16. Numerical model.

The experimental load and settlement results of the model experiment were projected onto the original project according to the similarity coefficient and compared with the numerical simulation results. Figure 17 shows a comparison of pile top settlements. The pile-top settlement results of the numerical simulations show a flat line without any obvious inflection point. The load corresponding to the settlement of 40 mm was taken as the ultimate load of the pile. The ultimate load was concentrated in the range of 280–367 MN. The ultimate bearing capacity of the model test pile was in the range of 320–440 MN, and the difference was approximately 15%.

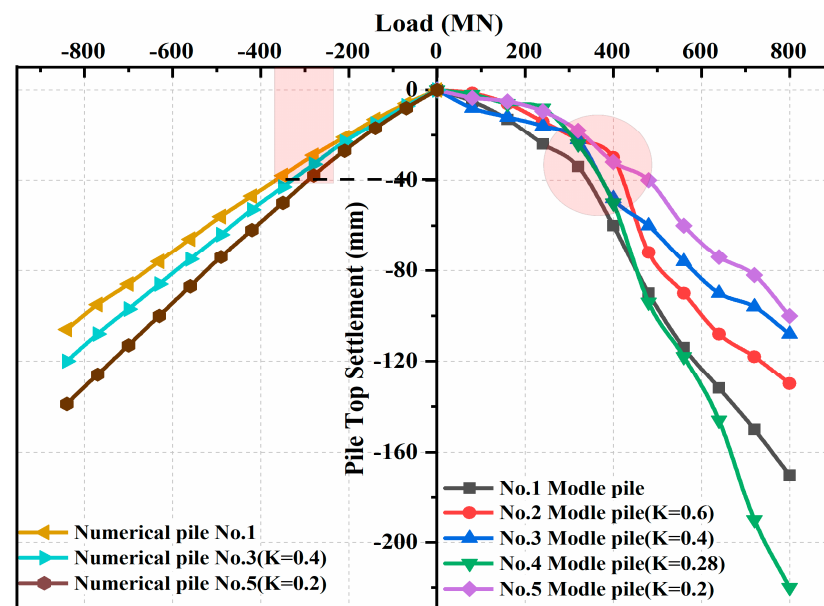


Figure 17. Comparison of pile-top settlements.

Even though the numerical simulation experiment process is too ideal and only serves as a guide for the regularity conclusion, the specific results of the model test shall prevail.

The numerical simulation experiments show the same trend as the model experiments. That is, the ultimate bearing capacity of the pile decreases with K . However, according to the provisions of the bearing capacity eigenvalues and irrespective of the numerical simulation experiments or model experiments, LDRPs with $K = 0.2-1$ can meet the same bearing capacity eigenvalue levels and have sufficient safety reserves.

The development law of pile compression in the numerical simulation experiments was the same as that in the model experiments.

Figure 18 shows a comparison of the results of the two experiments. Within the range of the ultimate bearing capacity of the pile, numerical simulation experiments show that pile compression increases with a decrease in K and wall thickness, T . The compression of the solid pile was the smallest, but that of the ring pile was large. With the increase in load, the difference between the compressions gradually became obvious. The overall law was consistent with the model experiments.

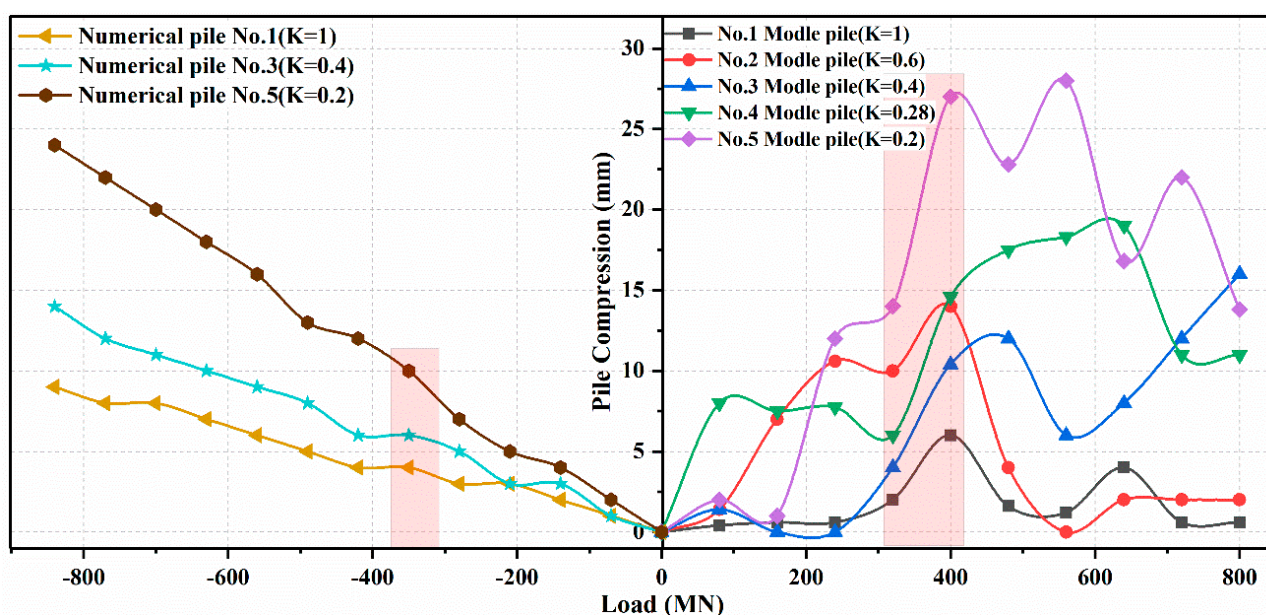


Figure 18. Comparison of pile compression.

5. Discussion

Due to the limitations of conditions, only one parameter, K , was researched in this paper. The physical and mechanical properties of LDRPs may be more accurately described if more parameters can be combined, such as the pile length, material, and back cover form. In addition, this study conducted only a vertical static load experiment of the pile. If the horizontal load and combined load can be increased, the mechanical response law of the LDRPs may be better summarized.

6. Conclusions

Variables in the LDRP mechanical property model experiments were strictly controlled. The similarity theory was used to compare LDRPs and LDSPs. We determined that LDRPs are distinguished by K , and the mechanical properties and bearing characteristics of LDRPs were revealed. The conclusions of this study are summarized below:

- (1) The smaller the value of K , the greater the settlement of the pile top, and the lower the ultimate bearing capacity of the LDRPs. The ultimate bearing capacity of the LDRPs with the same shape and size is the same as that of the LDSPs for a thickness-to-diameter ratio, K , in the range of 0.4–1; and for K in the range of 0.2–0.4, the bearing capacity is 80% that of a large-diameter solid pile. However, enough safety reserves remained.

- (2) The wall thickness and the stress area of the pile section decrease with K ; however, the compression of the pile increases. This is the main reason for the increase in the settlement of LDRPs.
- (3) The strain of the LDRPs increases with a decrease in K , but it is far less than the material strength of the pile. The position of the maximum pile strain moves up the pile as K decreases.
- (4) When $K = 0.2$, the large-diameter ring-shaped pile can save up to 64% of concrete usage. Despite this, the bearing capacity can reach 80% that of a large-diameter solid pile and has sufficient safety reserves.

Due to the limitations of conditions, only one parameter, K , was researched in this paper. The physical and mechanical properties of LDRPs may be more accurately described if more parameters can be combined, such as the pile length, material, and back cover form. In addition, this paper conducted only a vertical static load experiment of the pile. If the horizontal load and combined load can be increased, the mechanical response law of LDRPs may be better summarized.

Author Contributions: Conceptualization, A.Y. and Y.S.; methodology, Y.S.; software, L.D.; validation, Y.S., Y.L. and Y.G.; formal analysis, Y.S.; investigation, A.Y.; resources, L.D.; data curation, Y.L. and Y.G.; writing—original draft preparation, Y.S.; writing—review and editing, Y.S.; visualization, Y.S.; supervision, Y.S.; project administration, Y.S. All authors have read and agreed to the published version of the manuscript.

Funding: This research received no external funding.

Institutional Review Board Statement: Not applicable.

Informed Consent Statement: Not applicable.

Data Availability Statement: Not applicable.

Conflicts of Interest: The authors declare no conflict of interest.

References

1. Jiang, S.; Huang, M.; Fang, T.; Chen, W.; Shangguan, X. A new large step-tapered hollow pile and its bearing capacity. *Proc. Inst. Civ. Eng. Geotech. Eng.* **2020**, *173*, 191–206. [[CrossRef](#)]
2. Huang, M.; Jiang, S.; Xu, C.; Xu, D. A new theoretical settlement model for large step-tapered hollow piles based on disturbed state concept theory. *Comput. Geotech.* **2020**, *124*, 103626. [[CrossRef](#)]
3. Dong, Y.; Feng, Z.; He, J.; Chen, J. Bearing characteristics of large-diameter hollow composite pile. *J. Phys. Conf. Ser.* **2019**, *1168*, 022069. [[CrossRef](#)]
4. Zhang, Y.M.; Yan, Q.G. Comparative Study of Seismic Response of Solid Pile with Hollow Pile. *Appl. Mech. Mater.* **2011**, *94–96*, 1889–1893. [[CrossRef](#)]
5. Ruan, X. Practical Algorithm for large diameter pile tip bearing capacity based on displacement control. In Proceedings of the 6th International Conference on Energy and Environmental Protection (ICEEP 2017), Zhuhai, China, 29–30 June 2017; Kim, Y.H., Ed.; Atlantis Press: Amsterdam, The Netherlands, 2017; pp. 64–69. [[CrossRef](#)]
6. Xiao, S.; Wang, K.; Gao, L.; Wu, J. Dynamic characteristics of a large-diameter pile in saturated soil and its application. *Int. J. Numer. Anal. Methods Geomech.* **2018**, *42*, 1255–1269. [[CrossRef](#)]
7. Wang, H.; Wang, L.Z.; Hong, Y.; Zhu, R.H. Quantifying the influence of pile diameter on the load transfer curves of laterally loaded monopile in sand. *Appl. Ocean Res.* **2020**, *101*, 102196. [[CrossRef](#)]
8. Mankbadi, R.; Ramakrishna, A.; Yang, K.-Y. Reliability of pile driving analyzer for determination of axial capacity of large-diameter cylindrical pile: Case History. *Transp. Res. Rec.* **2010**, *2202*, 32–36. [[CrossRef](#)]
9. Liu, X.; Bai, X.; Zhang, M.; Evangelista, L. Load-Bearing Characteristics of Large-Diameter Rock-Socketed Piles Based on Ultimate Load Tests. *Adv. Mater. Sci. Eng.* **2020**, *2020*, 6075607. [[CrossRef](#)]
10. Yang, H.; Jiang, X.L.; Fu, J. Vertical Loading Test on the Bearing Capacity of Large-Diameter Filling-Piles in the Mudstone and Sandstone Foundation. *Adv. Mater. Res.* **2013**, *639–640*, 2195. [[CrossRef](#)]
11. Finn, W.L.; Dowling, J. Modelling effects of pile diameter. *Can. Geotech. J.* **2016**, *53*, 173–178. [[CrossRef](#)]
12. Deb, P.; Pal, S.K. Nonlinear analysis of lateral load sharing response of piled raft subjected to combined V-L loading. *Mar. Georesour. Geotechnol.* **2020**, *39*, 994–1014. [[CrossRef](#)]
13. GB 50007-2011; Code for Design of Building Foundation. Ministry of Construction of the People's Republic of China; China Construction Industry Press: Beijing, China, 2012.

14. Lv, Y.; Zhang, D. Geometrical effects on the load transfer mechanism of pile groups: Three-dimensional numerical analysis. *Can. Geotech. J.* **2017**, *55*, 749–757. [[CrossRef](#)]
15. Sinha, A.; Hanna, A.M. 3D Numerical Model for Piled Raft Foundation. *Int. J. Geomech.* **2016**, *17*, 04016055. [[CrossRef](#)]
16. Deb, P.; Pal, S.K. Structural and geotechnical aspects of piled raft foundation through numerical analysis. *Marine Georesour. Geotechnol.* **2022**, *40*, 823–846. [[CrossRef](#)]